CHEMISTRY OF MATERIALS

Article

pubs.acs.org/cm

Uniform Atomic Layer Deposition of Al_2O_3 on Graphene by Reversible Hydrogen Plasma Functionalization

René H. J. Vervuurt,[†] Bora Karasulu,[†] Marcel A. Verheijen,[†,‡] Wilhelmus (Erwin) M. M. Kessels,[†] and Ageeth A. Bol*[,†]

[†]Department of Applied Physics, Eindhoven University of Technology, P.O. Box 513, 5600 MB Eindhoven, The Netherlands
[‡]Philips Innovation Labs, High Tech Campus 11, 5656 AE Eindhoven, The Netherlands

Supporting Information

ABSTRACT: A novel method to form ultrathin, uniform Al_2O_3 layers on graphene using reversible hydrogen plasma functionalization followed by atomic layer deposition (ALD) is presented. ALD on pristine graphene is known to be a challenge due to the absence of dangling bonds, leading to nonuniform film coverage. We show that hydrogen plasma functionalization of graphene leads to uniform ALD of closed Al_2O_3 films down to 8 nm in thickness. Hall measurements and Raman spectroscopy reveal that the hydrogen plasma functionalization is reversible upon Al_2O_3 ALD and subsequent annealing at 400 °C and in this way does not deteriorate the graphene's charge carrier mobility. This is in contrast with oxygen plasma functionalization, which can lead to a uniform 5 nm thick closed film, but which is not reversible and leads to a reduction of the charge carrier mobility. Density functional theory (DFT) calculations attribute the uniform growth on both H_2 and O_2 plasma functionalized graphene to the enhanced adsorption of trimethylaluminum (TMA) on these surfaces. A DFT analysis of the possible reaction pathways for TMA precursor adsorption on hydrogenated graphene predicts a binding mechanism that cleans off the hydrogen functionalities from the surface, which explains the observed reversibility of the hydrogen plasma functionalization upon Al_2O_3 ALD.

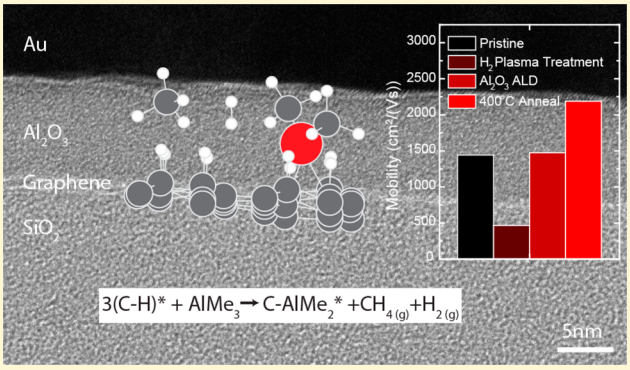

1. INTRODUCTION

Graphene is a two-dimensional (2D) material that has attracted significant interest in the scientific community due to its interesting electronic, optical, and thermal properties. The high carrier mobility of graphene and large maximum current density make it a promising candidate for postsilicon electronics.[1] The deposition of thin high-k dielectric films on graphene is required for many of these electronic applications. For example, radio frequency transistors require the deposition of dielectric layers on top of the graphene for good electrostatic control of the channel and better device reliability,[2,3] while lateral spin valves require ultrathin dielectrics on the graphene as a tunnel barrier.[4]

Atomic layer deposition (ALD) is the preferred method to deposit dielectric layers on graphene, due to its ability to deposit high quality and uniform materials with precise control of the layer thickness. However, the initiation of ALD growth on graphene is known to be a challenge due to the lack of out-of-plane bonds and surface hydrophobicity. ALD growth of dielectrics on pristine graphene therefore only occurs on defect sites or grain boundaries where dangling bonds or functional groups are present.[5,6] To overcome this issue different surface preparation techniques to initialize ALD growth on graphene have been investigated in the literature.[5−22] In general these techniques can be divided into three categories: 1) the use of seed-layers, such as self-assembled monolayers, polymers, evaporated metals (which are oxidized in air before ALD), and layers deposited by chemical vapor deposition (CVD),[5,10,22] 2) the creation of functional groups on the graphene surface by for example ozone[11] and plasma[12] treatments, and 3) tuning the underlying substrate to enhance the nucleation.[13]

The use of polymer seed-layers results in the conformal coverage of ALD oxide without damaging the graphene.[5,14,15] However, the polymer interlayer that is used has a low-k value, leading to a higher equivalent oxide thickness for the deposited polymer/oxide stack. Furthermore, the used polymers can dope the graphene, which results in a large Dirac-point shift of the created devices.[14] Oxidized metal seed-layers avoid these issues but trap charges at the graphene-dielectric interface. This deteriorates the mobility of graphene layers and reduces device performance.[10] The use of CVD layers to initialize growth does not affect the graphene properties but no longer offers the

Received: October 13, 2016
Revised: February 23, 2017
Published: February 23, 2017

DOI: 10.1021/acs.chemmater.6b04368
Chem. Mater. 2017, 29, 2090−2100

advantages of ALD in terms of thickness control, resulting in the deposition of thick layers (>10 nm).[22]

Degradation of the electrical properties of graphene is also observed for most covalent functionalization methods. This is because these methods rely on the conversion of sp^2-C bonds to sp^3 bonds, disrupting the 2D nature of graphene.[11,12,16,17] For example, ozone functionalization at 200 °C creates epoxy surface groups that enhance the nucleation of Al_2O_3 on graphene, yielding uniform Al_2O_3 growth on the graphene.[11] At the same time, however, these groups enhance the scattering of charge carriers in graphene, resulting in decreased carrier mobilities. To avoid this problem the ozone functionalization can be performed at lower temperatures. At temperatures below 50 °C, ozone is physisorbed on graphene leaving the sp^2 bonding intact. This prevents damaging the graphene and can even provide an improvement in the electrical properties of graphene following Al_2O_3 ALD.[18,19] The limited stability of physisorbed ozone on the graphene surface, however, also requires Al_2O_3 deposition at these low temperatures, decreasing the quality of the deposited films.[23]

The use of O_2 and N_2 plasmas to functionalize the graphene causes severe damage to the graphene, degrading its electrical properties.[12,16] To avoid this Shin et al. and Nourbakhsh et al. performed an O_2 plasma treatment on a sacrificial graphene layer.[20,21] This layer served as a nucleation layer for Al_2O_3 ALD that was either transferred onto a pristine graphene layer after the plasma exposure[20] or protected the underlying graphene during the plasma exposure.[21] With this method uniform Al_2O_3 layers down to 4 nm in thickness could be deposited without damaging the graphene. The requirement of an additional graphene transfer step, however, makes the process time-consuming and could trap polymer residues left over from the transfer procedure in between the layers.

To date H_2 plasmas have not been studied for the uniform growth of dielectric layers by ALD on graphene. The use of H_2 plasmas to initialize growth on graphene might be of interest because the H_2 plasma treatment (hydrogenation) has shown to be reversible.[24,25] The pristine graphene properties can be recovered after annealing the hydrogenated graphene in an Ar atmosphere at 400 °C. This might make it possible to directly grow ALD layers on hydrogen functionalized graphene, without the need for sacrificial layers or damaging the graphene, since the pristine graphene properties might be recovered after processing by an annealing step.

To this extent H_2 plasma pretreatments are investigated in this work to initialize Al_2O_3 ALD growth directly on graphene, without the use of a sacrificial layer. The ability of the H_2 plasma pretreatment to obtain uniform ALD growth on graphene is compared to O_2 plasma pretreatments and pristine graphene. The type of functional group created by the H_2 and O_2 plasma treatments is studied by X-ray photoelectron spectroscopy (XPS). The effects of the plasma treatments on the structural and electrical properties of the functionalized graphene is investigated by Raman and Hall measurements, before and after plasma treatment, after Al_2O_3 ALD, and after an anneal at 400 °C. Furthermore, the underlying reaction mechanism of the Al_2O_3 precursor adsorption on the functionalized graphene is investigated using *ab inito* calculations.

2. METHODOLOGY

2.1. Experimental Methods. Graphene samples (1 × 1 cm) were synthesized by CVD on Cu foil (Alfa Aesar 99.8%, No. 13382) of 25 μm. Before growth the Cu foil was cleaned using acetone, methanol, and a 30 s 1.0 M nitric acid (HNO_3) etch to remove the surface oxide. After rinsing in deionized water the Cu foil was dried and loaded into a tube furnace. The Cu foil was heated to 1050 °C under an Ar/H_2 (500/10 sccm) flow at a pressure of 0.4 Torr. After annealing the sample for 30 min, the H_2 flow was reduced to 6, and 100 sccm CH_4 was added to the gas flow for 20 min, resulting in a monolayer coverage of graphene on the Cu foil. The sample was cooled down to room temperature in 15 min while leaving the gas flows on.

The graphene on Cu was transferred to 90 nm SiO_2/Si (100) wafers by wet chemistry using poly(methyl methacrylate) (PMMA) A4 950k (Micro Chem.) as a support layer. Ferric chloride ($FeCl_3$ 0.1 M) was used to etch the Cu. After transfer the PMMA was removed using acetone with a final rinse in methanol. The samples were subsequently annealed at 400 °C in an Ar/H_2 atmosphere for 2 h, to minimize any PMMA residue remaining after PMMA lift-off.

The O_2 and H_2 plasma functionalization of the graphene was performed in an Oxford Instruments FlexAl reactor using a 100 W 50 mTorr plasma at 50 °C and a gas flow of 50 sccm O_2 or H_2, respectively. ALD was performed in the same reactor at 100 °C using trimethylaluminum (TMA) and H_2O. The timing sequence was as follows: (0.03 s, 4 s, 0,2 s, 10 s), (TMA, purge, H_2O, purge). After ALD one set of samples was annealed at 400 °C in an Ar/H_2 atmosphere for 2 h in a tube furnace.

The quality and electrical properties of the graphene samples were characterized before and after plasma treatment following ALD and after annealing with a Renishaw Invia Raman microscope (514.5 nm) and an Ecopia HMS-5300 Hall Effect Measurement System. The graphene samples used for the Hall measurements were approximately 1 × 1 cm^2 in size. Ohmic contact to the graphene was obtained by applying conductive silver paste at the corners of the graphene samples. The silver paint was applied before annealing the pristine graphene samples at 400 °C to exclude the influence of the annealing process on the contact formation. The formation of an Ohmic contact was confirmed by I−V measurements, which showed Ohmic behavior over the full measured range (−100−100 μA). The Hall measurements were performed at 25 °C under N_2 ambient. Prior to the measurements the samples were annealed at 150 °C for 10 min to remove any adsorbed H_2O from the graphene. Information on the surface groups created after plasma treatment was determined by a Thermo Scientific K-Alpha KA 1066 X-ray photon spectroscope (XPS). The uniformity of the deposited Al_2O_3 films was determined with a JEOL 7500 FA scanning electron microscope (SEM), a NT-MDT Solver P47 atomic force microscope (AFM), and a JEOL ARM 200 probe corrected transmission electron microscope (TEM), operated at 200 kV. A cross-sectional TEM sample from a Al_2O_3/graphene stack on a 90 nm SiO_2/Si wafer was prepared using the FIB lift-out method using a FEI Helios 650 DualBeam system. The thickness of the Al_2O_3 layer was determined by a J.A. Woollam M-2000D variable angle spectroscopic ellipsometer (SE).

2.2. Computational Methods. The binding energies of TMA on pristine, O_2, and H_2 plasma functionalized graphene were calculated by *ab initio* density functional theory (DFT). The calculations were performed using the projector augmented wave function (PAW)[26,27] as implemented in Vienna Ab Initio Simulation Package (*VASP* v.5.3.5).[28−31] The generalized gradient approximation (GGA) to DFT[32,33] was used with a plane-wave basis. The Perdew−Burke−Ernzerhof (PBE) exchange correlation functional[34,35] was used along with the DFT(PBE)-D3 method including the Becke-Jonson damping[36] to account for van der Waals interactions on an empirical basis. Eq 1 was used for computing the TMA adsorption (or, equivalently, binding) energies through physisorption (ΔE_p) or chemisorption (ΔE_c) on a given graphene surface

$$\Delta E_{p/c} = E_{PG} - E_P - E_G \quad (1)$$

where E_{PG} is the total energy of the physisorbed/chemisorbed complex of the TMA precursor with graphene, and E_P and E_G are the (gas phase) total energies of the isolated precursor and the graphene surface under consideration. Relevantly, the (reaction) energies ($\Delta E_r = \Delta E_c - \Delta E_p$) required for converting the corresponding physisorbed

DOI: 10.1021/acs.chemmater.6b04368
Chem. Mater. 2017, 29, 2090−2100

species into chemisorbed ones, e.g. via dissociation of the given precursor on the given surface, are also presented. Gibbs free energy changes ($\Delta G = \Delta(E_{elec} + E_{ZPE}) - T\Delta S$) associated with TMA adsorption were estimated in the ideal gas limit at the typical ALD conditions (T = 100 °C and P = 100 mTorr), accounting for the translational, rotational, and vibrational contributions to the enthalpy and entropy terms. All-atom vibrational analyses were performed using the finite differences method implemented in *VASP*. Further details about the computational calculations can be found in the Supporting Information and elsewhere.[37]

3. RESULTS AND DISCUSSION

3.1. Surface Species Analysis by XPS. First the effect of the O_2 and H_2 plasma functionalization on graphene was studied by XPS to analyze the surface groups created during the plasma exposure. Before plasma exposure, the pristine graphene samples were annealed at 400 °C for 2 h in Ar/H_2 (5%) atmosphere for 2 h. This was done to minimize any polymer residues left on the surface after transfer and ensure the cleanest graphene possible. In the case of the O_2 plasma treatment an exposure time of 30 s was chosen, while for the H_2 plasma 35 s was used, both at a pressure of 50 mTorr and plasma power of 100 W. These are the optimal exposure times; longer exposures resulted in irreversibly damaging the graphene as confirmed by Raman spectroscopy, whereas shorter exposures did not result in a closed Al_2O_3 layer (see discussion in the Supporting Information and Figure S1).

The XPS measurements of the C 1s spectra of graphene after a 30 s O_2 plasma treatment and a 35 s H_2 plasma treatment are shown in Figure 1. As a reference the spectrum of pristine graphene after transfer to 90 nm SiO_2 and 400 °C anneal is also shown in Figure 1. The main peak contributing to the C 1s spectrum of pristine graphene (Figure 1a) is located at 284.4 eV and originates from the sp^2 bonding of the carbon atoms. The weak peak at 286.4 eV corresponds to C−O bonding. These C−O bonds are commonly seen on the graphene basal plane and originate from grain boundaries or defects sites[38,39] or are the result of polymer residues remaining on the graphene after its transfer to SiO_2 and annealing.[40] In addition, two plasmon loss features observed at 290.4 and 293.2 eV are caused by the interaction of the photoelectron with free electrons present in the graphene.[41]

After a 30 s O_2 plasma treatment (Figure 1b) the amount of C−O bonds increases, indicating the creation of epoxide groups (C−O−C) or hydroxide (C−OH) containing surface groups on the graphene. Two additional peaks appear in the spectrum compared to that of pristine graphene. The peak at 284.6 eV is related to sp^3 bonding of the carbon atoms. This is combined with a decrease in sp^2 bonding, which indicates that the O_2 plasma treatment indeed disrupts the sp^2 structure of the graphene.[41] The second peak appears at 289.0 eV and is related to the creation of C═O bonds, possibly in the form of carbonyl groups. Since carbonyl groups can only be formed in-plane due to their sp^2 carbon constituent, these are most likely located at defects or edge sites of the graphene basal plane. The plasmon loss features can no longer be observed after the O_2 plasma treatment. This is likely due to the deterioration of the electrical properties of the graphene after the plasma exposure. The O 1s spectra of the graphene samples did not provide any additional information on the C−O and C═O bonding due to the dominating contribution from the SiO_2 substrate to the O 1s signal.

After a 35 s H_2 plasma treatment (Figure 1c) the graphene shows a strong increase in the sp^3 bonding, combined with a decrease in the sp^2 bonding. This is most likely related to the formation of C−H bonds (hydrogenated graphene),[24] which cannot be observed by XPS. A distinct hallmark of hydrogenated graphene is the reversibility of hydrogenation upon annealing at 400 °C.[25] This reversibility can be confirmed by Raman spectroscopy.[24,25] After hydrogenation the Raman D-band at 1350 cm^{-1}, which is related to defects or sp^3 bonding of the carbon atoms, can be observed. This band disappears after annealing at 400 °C in Ar atmosphere, indicating that hydrogen atoms desorb from the graphene surface at this temperature and the original graphene sp^2 configuration is restored. This reversibility of the D-band is also observed for the 35 s H_2 plasma treated sample in this work (see below), indicating that the graphene is indeed hydrogenated upon H_2 plasma exposure.

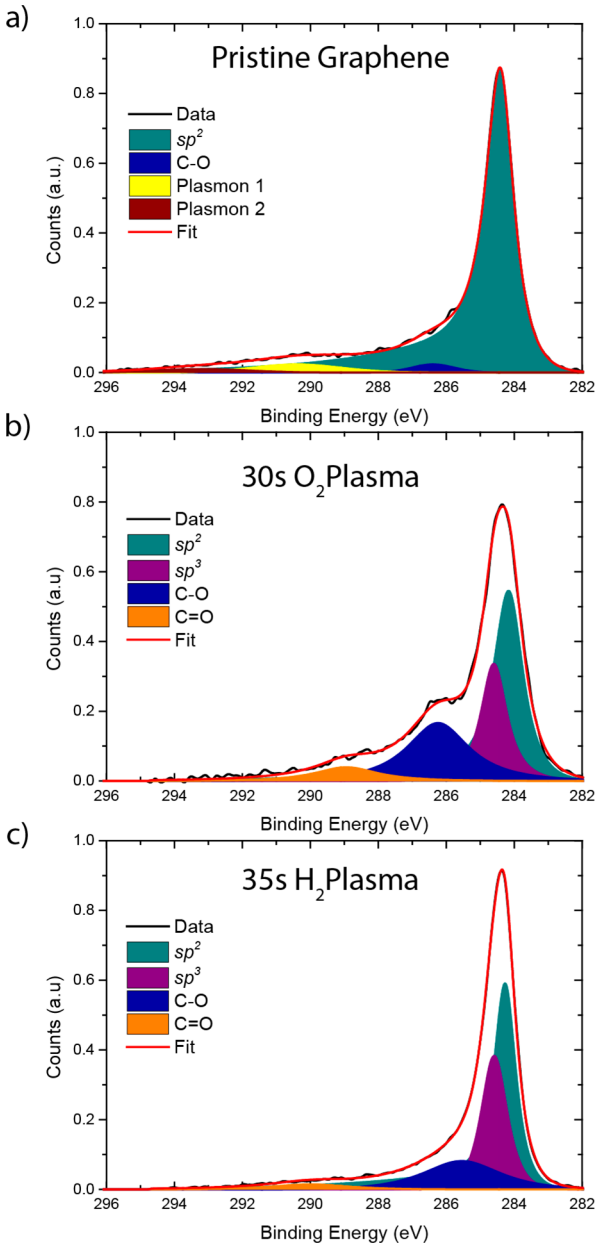

Figure 1. XPS spectra of the core level C 1s of a) pristine graphene (after transfer to SiO_2), b) graphene after a 30 s O_2 plasma treatment, and c) graphene after a 35 s H_2 plasma treatment at a pressure of 50 mTorr and a plasma power of 100 W.

DOI: 10.1021/acs.chemmater.6b04368
Chem. Mater. 2017, 29, 2090−2100

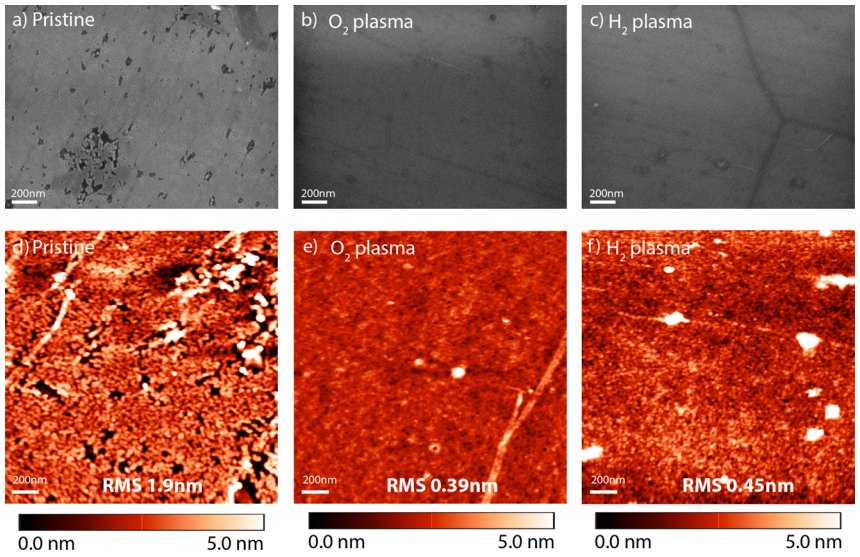

Figure 2. SEM and AFM images showing the Al_2O_3 coverage on graphene after 100 cycles of Al_2O_3 ALD at 100 °C for a,d) pristine, b,e) 30 s O_2 plasma, and c,f) 35 s H_2 plasma treated graphene. The root-mean-square (RMS) roughness determined from the AFM measurements is indicated as well.

Apart from a change from sp^2 to sp^3 bonding the XPS also shows an increase in the C−O bonding after the H_2 plasma treatment. This could be due to the formation of hydroxyl groups upon H_2 plasma exposure or adventitious carbon. The hydroxyl groups could be formed by residual water desorbing from the reactor walls and dissociating in the plasma, whereas the adventitious carbon could be formed due to carbon containing molecules present in the air adsorbing on the sample during transfer to the XPS system. Summarizing, the XPS results indicate that an O_2 plasma creates a combination of epoxide, hydroxide, and carbonyl groups on the graphene surface. A hydrogen plasma most likely results in the creation of C−H groups with some hydroxyl impurities.

3.2. Al_2O_3 ALD Growth on Functionalized Graphene. To investigate the effect of the created functional groups on the uniformity of the Al_2O_3 nucleation, 100 ALD cycles were performed on the plasma treated samples. A pristine graphene sample was added to the deposition as a reference. The uniformity of the Al_2O_3 after deposition, determined by SEM and AFM, is shown in Figure 2. On the pristine graphene reference sample no uniform growth is obtained (Figure 2a,d). Small holes and a granular Al_2O_3 structure are visible in both the AFM and SEM images. The roughness, determined from an average of three AFM scans ($2 \times 2\ \mu m^2$), is 1.9 ± 0.1 nm for the pristine graphene sample after Al_2O_3 ALD. Both the 30 s O_2 plasma (Figure 2b,e) and the 35 s H_2 plasma (Figure 2c,f) treated graphene show uniform deposition of Al_2O_3. No pinholes are visible, and the roughness is considerably lower, 0.39 ± 0.05 nm and 0.45 ± 0.05 nm for the O_2 and H_2 plasma, respectively, indicating that a closed Al_2O_3 layer is obtained. The surface groups created on the graphene with the O_2 and H_2 plasma pretreatments thus sufficiently increase the ALD precursor adsorption on graphene, enhancing the nucleation of Al_2O_3 ALD and enabling uniform Al_2O_3 growth on graphene.

The thicknesses of the Al_2O_3 layers deposited on the O_2 and H_2 plasma treated graphene have been determined with spectroscopic ellipsometry (SE) to be 11 ± 1 nm and 9 ± 1 nm, respectively. The higher thickness of the Al_2O_3 on the O_2 plasma treated sample indicates a shorter nucleation delay of the Al_2O_3 when an O_2 plasma treatment is used. This is most likely caused by a more favored adsorption of TMA precursor molecules on epoxide (C−O−C) and hydroxyl (C−OH) groups compared to hydrogen groups (C−H). This will be discussed in more detail in the DFT section of this paper. The shorter nucleation delay on O_2 plasma treated graphene also makes it possible to deposit thinner uniform Al_2O_3 layers on the O_2 treated samples (see Figure S2). In the case of the O_2 plasma treated graphene, the Al_2O_3 layer was already closed after 50 cycles, corresponding to a layer thickness of approximately 5 nm. Considering the H_2 plasma treated samples, pinholes were still present in the layer after 75 ALD cycles (see Figure S2). This indicates that 100 ALD cycles is the minimum required for a closed Al_2O_3 layer using H_2 plasma functionalization with the current plasma settings and exposure time. Increasing the H_2 plasma exposure time could help to increase the coverage at lower ALD cycles numbers but can also irreversibly damage the graphene (see discussion in the Supporting Information).

To confirm that the Al_2O_3 layer after a H_2 plasma treatment and 100 cycles Al_2O_3 ALD is indeed closed, a TEM cross-section was made (Figure 3). The cross-section shows a uniform Al_2O_3 layer with a thickness of 7.8 ± 0.4 nm, which is in agreement with the Al_2O_3 thickness obtained from the SE measurements.

3.3. Quality of the Graphene: Raman Characterization. The above results show that uniform Al_2O_3 deposition

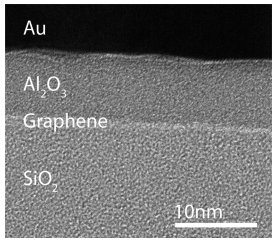

Figure 3. Cross-sectional TEM image of 100 cycles of Al_2O_3 deposited on graphene treated with 35 s H_2 plasma. The Al_2O_3 layer is 7.8 ± 0.4 nm thick and pinhole-free.

DOI: 10.1021/acs.chemmater.6b04368
Chem. Mater. 2017, 29, 2090−2100

on graphene can be obtained by using an O_2 and H_2 plasma pretreatment. However, it is generally observed that graphene is damaged by such treatments.[12,16,20,21] This is also indicated by the XPS data in Figure 1, which show the conversion of sp^2 bonds to sp^3 bonds. In this regard, the quality of the graphene was studied before the plasma treatment, after the plasma treatment, after ALD, and after annealing at 400 °C using Raman spectroscopy and Hall measurements (next section). The Raman measurements performed after each processing step for the different graphene samples are shown in Figure 4. The Raman D-band (~1350 cm^{-1}) is related to defects in the graphene or to the functionalization of graphene by covalent bonding.[42] Pristine graphene (Figure 4a) shows no D-band indicating that the graphene is of high quality. Subsequent Al_2O_3 ALD on the pristine graphene does not create any defects in the graphene but also does not result in the formation of a closed Al_2O_3 layer. Annealing the pristine graphene with Al_2O_3 at 400 °C for 2 h in a 50:1 Ar/H_2 mixture results in the formation of a small D-band and an α-carbon background (~1200−1500 cm^{-1}), which could be due to the dehydrogenation of the polymer residues present at the graphene surface. These residues are a result of the graphene transfer process.[40] Even though the graphene was annealed before ALD to minimize the residues, it has appeared impossible to remove them completely.[40]

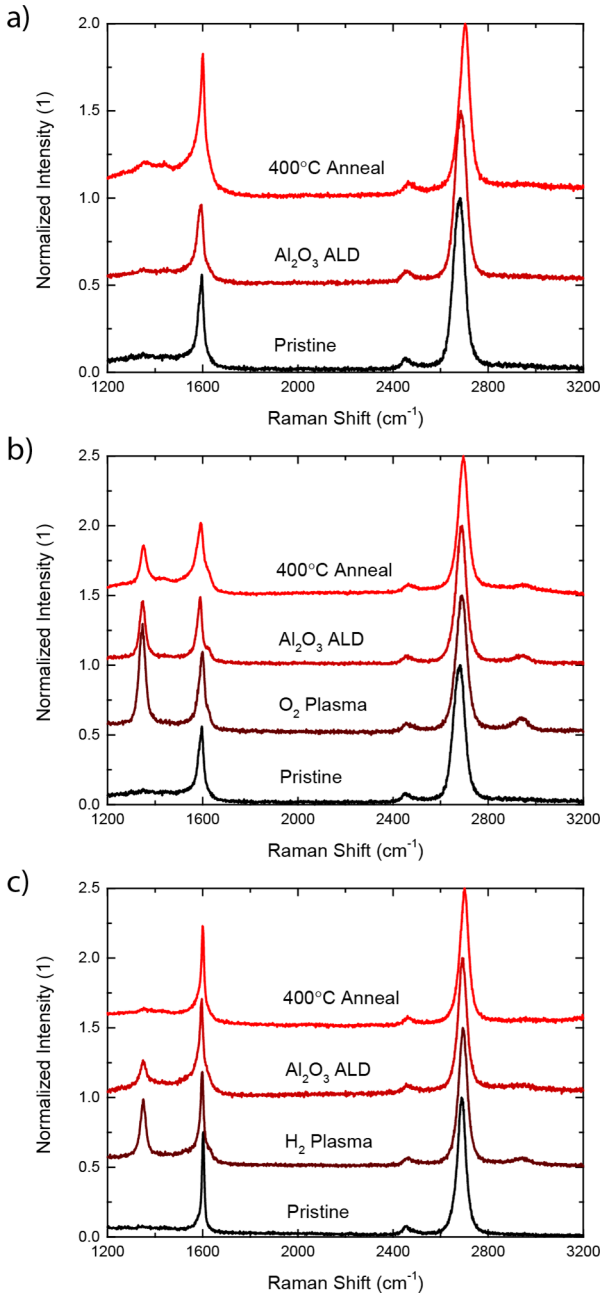

Figure 4. Raman spectra of the different graphene samples after each processing step: transfer, plasma treatment, 100 cycles Al_2O_3 ALD, and 400 °C anneal for a) untreated graphene, b) 30 s O_2 plasma treated graphene, and c) 35 s H_2 plasma treated graphene. The spectra are normalized to the 2D band and are offset for clarity.

Treating the graphene with a 30 s O_2 plasma creates a significant D-band (Figure 4b) as a result of the conversion of sp^2 to sp^3 carbon (also shown by XPS) and possibly by the creation of defects due to ion bombardment. After Al_2O_3 ALD the magnitude of the D-band decreases considerably, indicating that the ALD process is able to partially heal the defects introduced by the plasma pretreatment or remove functional groups present on the graphene. This could be due to a reaction of the ALD precursor molecules with the functional groups or the passivation of defects by Al_2O_3.[43] In an attempt to further reduce the D-band, the sample was annealed at 400 °C under the same conditions as the pristine graphene. Although this reduced the D-band further, it could not be completely removed. Possibly, the species in the O_2 plasma irreversibly damaged the graphene, or part of the functional groups remains on the graphene.

In the case of a 35 s H_2 plasma treatment, a similar trend as for the O_2 plasma treated sample can be observed by Raman spectroscopy (Figure 4c). Similar to the O_2 plasma the H_2 plasma results in the appearance of a D-band in the Raman spectrum. The D-band after H_2 plasma treatment is lower compared to the D-band created after O_2 plasma treatment. Subsequent Al_2O_3 ALD leads to a reduction of these defects or removal of the C−H functional groups from the surface. Annealing the H_2 plasma treated sample with Al_2O_3 at 400 °C results in the complete annihilation of the D-band. The Raman spectrum obtained after annealing is similar to the pristine graphene spectrum obtained after transfer to the SiO_2 substrate. This points in the direction that the D-band is indeed related to C−H bonds, which can be removed after annealing at 400 °C, as defects are not likely to be annealed at this temperature.[24] It should be noted that for hydrogenated graphene also a weak D′-band (~1620 cm^{-1}) should be present.[42] This peak is however not distinguishable in Figure 4c, because the G-band (~1600 cm^{-1}) is significantly broadened upon annealing the pristine graphene to remove the PMMA residue, thus introducing overlap with the D′ band. This broadening is related to the formation of small amounts of amorphous carbon during the anneal on top of the graphene.[44] Direct H_2 plasma exposure of pristine graphene (without annealing) does result in the formation of a distinguishable D′-band (data not shown).

3.4. Quality of the Graphene: Hall Mobility Characterization. Hall mobility measurements were performed to investigate the effect of the O_2 and H_2 plasma treatments on the electrical properties of graphene (Figure 5). The mobility values of the pristine graphene samples used in this study range between 1300 and 1800 $cm^2/(V\ s)$ (indicated by the black bars in Figure 5) which is typical for large area (1 × 1 cm^2) CVD graphene.[3,45,46] The deposition of Al_2O_3 on pristine graphene results in a mobility increase to 117% of its initial value (1520

DOI: 10.1021/acs.chemmater.6b04368
Chem. Mater. 2017, 29, 2090−2100

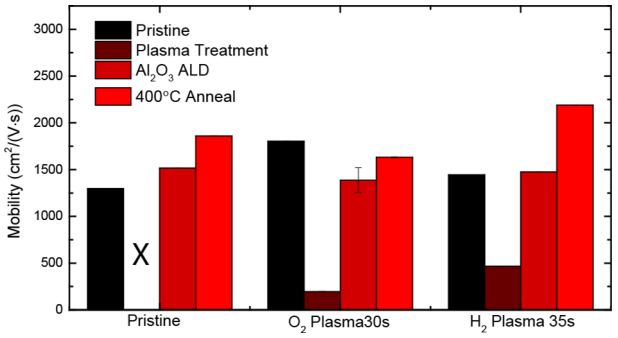

Figure 5. Mobility of graphene determined by Hall measurements, after transfer, after plasma treatment, after 100 cycles Al_2O_3 ALD, and after 400 °C anneal for pristine, O_2, and H_2 plasma treated graphene.

$cm^2/(V\ s)$). This increase could be caused by several effects: (1) Al_2O_3 can passivate defects present in the graphene;[47] (2) Al_2O_3 can act as a barrier preventing H_2O and O_2 reaching the graphene surface which would otherwise degrade the carrier mobility of graphene;[48] (3) The Al_2O_3 layer can also help to screen charged impurities, present in the SiO_2 substrate, which would normally act as scattering centers for the electrons and holes in the graphene.[49] Charge screening could also explain why the mobility is further increased to 140% of its initial value (1860 $cm^2/(V\ s)$) after the sample is annealed at 400 °C. This is because annealing Al_2O_3 at 400 °C generally gives the highest Al_2O_3 built-in charge,[50] resulting in maximum passivation and an increased mobility of the graphene after annealing. It should be noted though that the Al_2O_3 layer on pristine graphene is not closed and therefore not suited for applications, for example as a gate dielectric.

Figure 5 also shows that both the O_2 and H_2 plasma treatments reduce the charge carrier mobility of graphene, as expected. After O_2 plasma the mobility is reduced to 195 $cm^2/(V\ s)$ (11% of its initial value), whereas after a H_2 plasma the mobility is decreased to 467 $cm^2/(V\ s)$ (32% of its initial value). This is in line with the XPS and Raman data which show the conversion of sp^2 to sp^3 carbon. The out-of-plane bonds act as scattering centers for the electrons and holes in the graphene and therefore lower the mobility.

Al_2O_3 ALD on the O_2 plasma treated sample causes a partial recovery of the mobility to 78% of its initial value (1390 $cm^2/(V\ s)$), most likely due to passivation and barrier properties of Al_2O_3, as was discussed for ALD on pristine graphene above. Additionally, part of the functional groups or defects might be removed from the surface by the precursor molecules during Al_2O_3 ALD. This hypothesis is further strengthened by the observed decrease of the D-band in the Raman spectrum after Al_2O_3 ALD (Figure 4b). The DFT section of this paper will elaborate further on this hypothesis. The charge carrier mobility of the O_2 plasma treated graphene sample with Al_2O_3 can be recovered to 91% of its original value (1630 $cm^2/(V\ s)$) by annealing at 400 °C. The recovery is most likely a result of the improved passivation properties of the Al_2O_3, as observed for the pristine sample. Additionally, some functional groups on the graphene desorb during the annealing, indicated by a further decrease in the Raman D-band (Figure 4b). The functional groups removed could be primarily hydroxyl groups, which have limited stability on graphene (see discussion in the DFT section). The incomplete recovery of the mobility after annealing indicates that some defects or functional groups remain on the O_2 plasma treated sample, which is confirmed by the still observable D-band in the Raman spectra.

Al_2O_3 ALD on the H_2 plasma treated graphene results in a large mobility improvement from 32% (467 $cm^2/(V\ s)$, after the H_2 plasma treatment) to 102% of its initial value (1470 $cm^2/(V\ s)$, after 100 ALD cycles). As for the O_2 plasma treatment, this recovery is most likely caused by a combination of the passivation and barrier properties of Al_2O_3 and a partial removal of the surface groups. Likewise, the removal of surface groups is supported by the decrease of the D-band in the Raman spectrum after Al_2O_3 ALD (Figure 4c). Compared to the O_2 plasma treatment, the D-band is considerably weaker for the H_2 plasma treatment after ALD, indicating that the groups created by the H_2 plasma treatment can be more easily removed, which explains the higher mobility recovery. Annealing the sample at 400 °C further improves the mobility to 152% of its original value (2190 $cm^2/(V\ s)$). The absence of a D-band in the Raman spectrum after annealing the H_2 plasma treated samples explains the larger increase of the mobility compared to the O_2 treatment. This also shows that the H_2 plasma treatment is fully reversible and that the functional groups created by the plasma treatment can be removed by a 400 °C anneal.

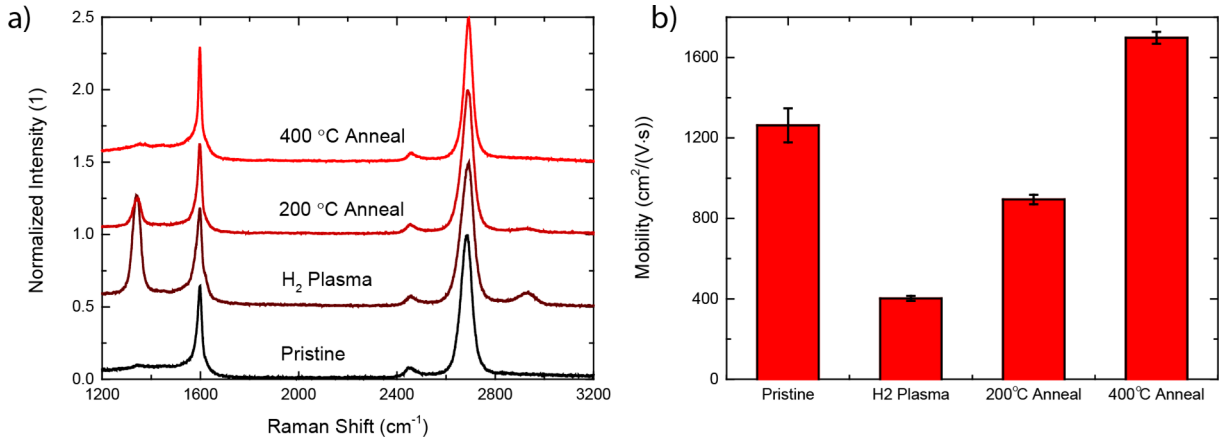

Figure 6. Hydrogen plasma reversibility for a graphene sample exposed for 35 s to H_2 plasma and annealed at 200 and 400 °C. a) Raman spectra and b) mobility determined from Hall measurements after the different processing steps. The pristine graphene sample was annealed at 400 °C before the Hall measurement to exclude the influence of annealing effects on the mobility.

DOI: 10.1021/acs.chemmater.6b04368
Chem. Mater. 2017, 29, 2090−2100

Table 1. Computed (PBE-D3 Level) Physisorption (ΔE_p), Chemisorption (ΔE_c), and Reaction ($\Delta E_r = \Delta E_c - \Delta E_p$) Energies (in eV) of TMA on Bare and Functionalized Graphenes[a]

system	coverage	ΔE_p	ΔE_c	ΔE_r	type
Pristine Graphene (PG)	0%	−0.53 [−0.23]	1.84 [2.29]	2.37 [2.52]	Me transfer (1a)
Graphene Oxide (GO)					
GO − epoxidized (single-sided)	25%	−1.70 [−1.04]	−7.37 [−6.82]	−5.67 [−5.78]	Me_2 release (1b)
			−5.69 [−5.15]	−3.99 [−4.11]	Me transfer (1a)
GO − hydroxylated (double-sided)[b]	50%	−0.45 [−0.34]	−2.67 [−2.56]	−2.22 [−2.22]	CH_4 release (2a)
GO − random mixture (single-sided) (epoxy + hydroxyl + hydrogen groups)	33%	−0.61 [−0.16]	−5.33 [−4.76]	−4.72 [−4.60]	Me_2 release (1b)
			−3.52 [−3.21]	−2.91 [−3.05]	CH_4 release (2a)
Hydrogenated graphene (HG)					
HG − stirrup (single-sided)	25%	−0.54 [−0.11]	−0.54 [0.01]	0.00 [0.12]	CH_4 release (2a)
			−1.29 [−1.20]	−0.75 [−1.09]	H_2 release (2b)
			−2.23 [−2.20]	−1.69 [−2.09]	$H_2 + CH_4$ release (2c)
			−0.38 [−0.19]	0.16 [−0.08]	$H_2 + Me_2$ release (2d)
HG − honeycomb (single-sided)	25%	−0.44 [−0.07]	0.12 [0.42]	0.56 [0.49]	CH_4 release (2a)
			−1.00 [−0.93]	−0.56 [−0.86]	H_2 release (2b)
			−1.39 [−1.48]	−0.95 [−1.41]	$H_2 + CH_4$ release (2c)
			0.25 [0.13]	0.69 [0.20]	$H_2 + Me_2$ release (2d)

[a]Corresponding Gibbs free energy changes (ΔG) are given in brackets. ΔE_c values are only reported for the lowest-energy chemisorbed species, as identified by "Type" (see eqs 2−3 for definitions). The coverage is defined as the relative ratio of the number of H and/or O adatoms to the carbon atoms on graphene. [b]The single-sided hydroxylated graphene oxide is not stable upon TMA binding (i.e., the −OH groups leave the surface) and thus not included in this table.

The additional improvement of the mobility observed after Al_2O_3 ALD and annealing for the H_2 treated sample compared to the pristine graphene sample (152% vs 140%) could be caused by the removal of polymer residues from the graphene surface during the plasma exposure. To investigate this possible cleaning effect, a graphene sample, which was first annealed at 400 °C, was hydrogenated and subsequently annealed at 200 °C for 2 h and 400 °C for 2 h without performing Al_2O_3 ALD (Figure 6). Raman spectroscopy (Figure 6a) shows that after annealing at 400 °C the graphene is recovered to its original state without functionalization. Figure 6b shows that this is accompanied by an increase in the mobility to 134% of its original value. This indicates that the H_2 plasma indeed removes polymer residuals from the surface and explains the additional improvement observed compared to pristine graphene.

The removal of polymer residues possibly also occurs during the O_2 plasma treatment.[19] However, no mobility improvement is observed for the O_2 plasma sample. Most likely, the mobility decrease due to the remaining functional groups is larger than the mobility increase due to polymer residue removal.

3.5. DFT Simulations. To further understand the enhanced Al_2O_3 nucleation on O_2 and H_2 plasma treated graphene first-principles (*ab initio*) DFT simulations were performed. To this end, models of pristine, oxygenated graphene (graphene oxide), and hydrogenated graphene were created (Figure S3). In principle functional groups can be attached to one or both facets of graphene, leading to single-sided or double-sided functionalization. However, one should note that graphene is placed on a Si/SiO_2 substrate during the O_2/H_2 plasma pretreatments, and the functionalities will therefore be predominantly attached to the accessible side rather than both sides. In view of this, the current DFT analysis is limited to the single-sided varieties (unless stated otherwise). Besides, the SiO_2 substrate is shown to only have a very limited effect on the TMA precursor adsorption (see the SI, Section 5). Considering this and the concomitant computational efforts, the SiO_2 substrate was not included in the simulation models used for the further analysis.

Pristine graphene (PG) was modeled by an 8 × 8 graphene supercell. For graphene oxide (GO) several models were considered accounting for the different oxygen-containing surface groups observed by XPS (Figure 1). Unlike epoxidized graphene, it turned out that single-sided hydroxylated graphene was not stable upon TMA binding due to the detaching −OH groups, as evident from the molecular dynamics simulations at finite temperature (data not shown). Therefore, double-sided hydroxylated graphene was used to simulate the TMA binding on hydroxylated graphene. In contrast, the hydroxyl groups were stable on the single-sided GO mixture, containing nonordered decoration of epoxy, hydroxyl, and hydrogen. For hydrogenated graphene (HG), the two most-likely configurations of the single-sided HG were modeled. A detailed discussion regarding the choice of these models can be found in the Supporting Information (HG) and elsewhere (PG and GO).[37]

The TMA precursor physisorption (ΔE_p), chemisorption (ΔE_c), and reaction energies ($\Delta E_r = \Delta E_c - \Delta E_p$) were calculated for each of the model systems. For computing the chemisorption energies, several reaction pathways were considered

$$2X^* + AlMe_{3(g)} \rightarrow X{-}AlMe_2^* + X{-}Me^* \quad (2a)$$

$$2X^* + AlMe_{3(g)} \rightarrow X_2{-}AlMe^* + Me_{2(g)} \quad (2b)$$

$$2X^* + AlMe_{3(g)} \rightarrow X_2{-}AlMe{-}CH_2^* + CH_{4(g)} \quad (2c)$$

$$(X{-}H)^* + AlMe_{3(g)} \rightarrow X{-}AlMe_2^* + CH_{4(g)} \quad (3a)$$

$$2(C{-}H)^* \rightarrow (C{-}C)^* + H_{2(g)} \quad (3b)$$

DOI: 10.1021/acs.chemmater.6b04368
Chem. Mater. 2017, 29, 2090−2100

$$3(X{-}H)^* + AlMe_{3(g)} \rightarrow X{-}AlMe_2^* + 2X^* + CH_{4(g)} + H_{2(g)} \quad (3c)$$

$$2(X{-}H)^* + AlMe_{3(g)} \rightarrow X_2{-}AlMe^* + Me_{2(g)} + H_{2(g)} \quad (3d)$$

where X represents either C or O, depending on the functionalization type (pristine or oxygenated). In addition, X−H denotes that the surface site is H-terminated and an asterisk refers to a surface group, whereas Me stands for a methyl ($-CH_3$) group. Other reaction pathways are possible depending on the ALD temperature, simultaneous binding of multiple precursors, and lingering coreactants/contaminants, etc. However, the approach used here provides sufficient information for a qualitative comparison of the binding energies and is commonly used for studying ALD processes on graphene[37,51,52] and other substrates.[53,54]

The results of TMA physisorption and chemisorption on the different graphene model systems are compiled in Table 1, whereas the corresponding minimum-energy structures of the physisorbed and chemisorbed species for the most relevant pathways are shown in Figure 7. A complete overview of all considered reaction pathways can be found in the Supporting Information (Figure S4).

Pristine graphene has a high chemical stability due to the sp^2-carbon configuration. This results in a rather weak TMA physisorption (ΔE_p = −0.53 eV) accompanied by an unfavorable (endothermic) chemical binding of TMA (ΔE_c = 1.84 eV). The dissociative TMA binding preferably proceeds via a methyl transfer mechanism (eq 2a), which involves a high activation energy (ΔE_a = 3.60 eV, see Figure S5 for the minimum-energy path). The other investigated reaction pathways do not lead to Al bonding on the graphene (Figure S4) which is required for proper Al_2O_3 nucleation. This indicates that TMA adsorption on PG is kinetically and thermodynamically unfavorable, which is in agreement with the SEM and AFM results (Figure 2a,d), showing nonuniform coverage of Al_2O_3 on pristine graphene. Nucleation probably starts at defect sites and grain boundaries with enhanced chemical reactivity, while no growth occurs on the pristine graphene. This results in the observed island-like growth instead of a uniform smooth Al_2O_3 layer due to the unfavorable TMA adsorption on the graphene plane.

Graphene oxide, however, can facilitate uniform nucleation and growth for Al_2O_3 ALD (Figure 2b,e and also elsewhere[20,21]). In line with this, the DFT calculations indicate a stronger TMA adsorption on all considered GO surfaces, compared to PG (Table 1, Figure S3). Stronger TMA adsorption on GO can be attributed to the availability of p-orbitals of the surface oxygen that interact with those of TMA aluminum. Among the different models, GO with ordered epoxy groups provides the strongest adsorption of TMA, due to having the highest free-electron density. High binding affinities are obtained for epoxidized GO, as evident from the physisorption and chemisorption energies (ΔE_p = −1.70 eV and ΔE_c = −7.37 eV). Compared to epoxidized GO, hydroxylated GO provides a weaker TMA adsorption (ΔE_p = −0.45 eV and ΔE_c = −2.67 eV), likely due to the H-passivation effect (i.e., reduced availability of free-electrons) of the oxygen. Likewise, a mixture of these two oxygen-containing functionalities provides an intermediate TMA binding strength (ΔE_p = −0.61 eV and ΔE_c = −5.33 eV). Considering the DFT calculations, it becomes clear that O_2 plasma pretreatments

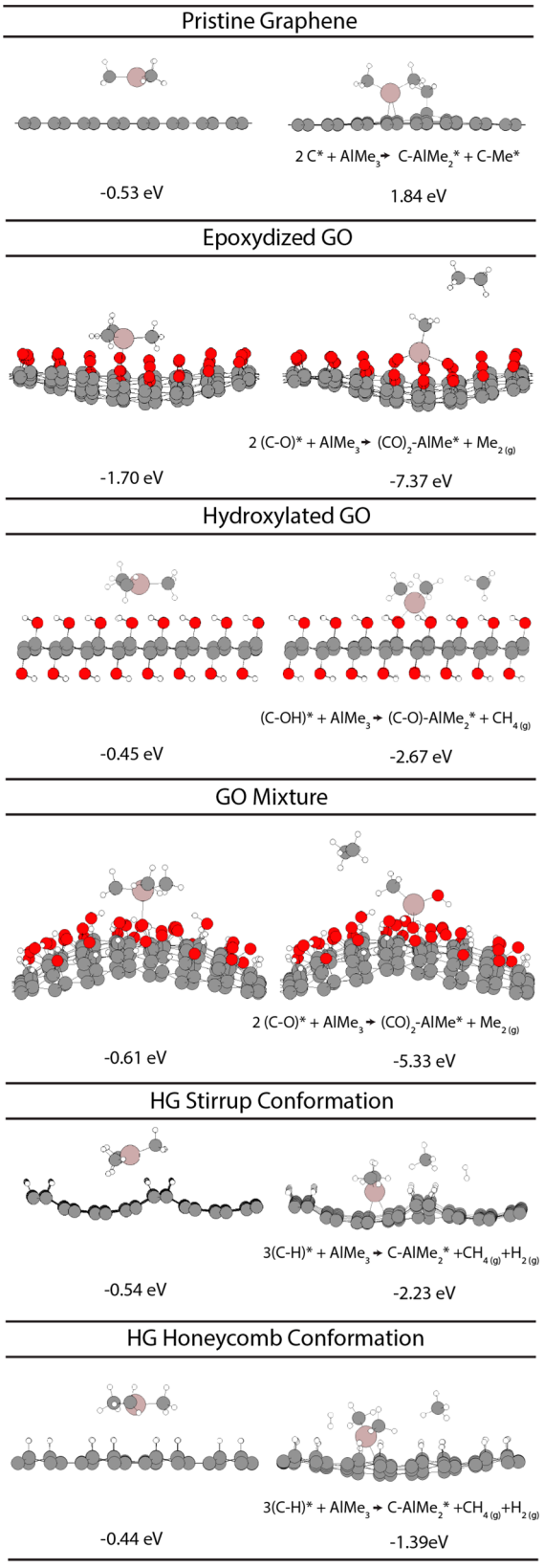

Figure 7. DFT-predicted structures of the lowest-energy (left) physisorbed and (right) chemisorbed species and their relative energies from the TMA adsorption on pristine graphene, oxygenated graphene (i.e., graphene oxide, GO), and hydrogenated graphene (HG).

DOI: 10.1021/acs.chemmater.6b04368
Chem. Mater. 2017, 29, 2090−2100

enable an improved ALD nucleation by predominantly attaching epoxy groups which have a strong binding affinity toward TMA.

From the analysis of the energetically most plausible pathways predicted for the TMA chemisorption on the GO surfaces (Table 1 and Figure 7), a variation depending on the surface functionalization can be observed. On single-sided epoxidized GO, TMA preferably chemisorbs trifunctionally (through three surface epoxys) while releasing a volatile ethane (Me_2 or C_2H_6) product (eq 2b, Figure 7). The latter proceeds with a negligible barrier (ΔE_a = 0.04 eV, Figure S6), while gaining substantial energy in return (ΔE_c = −7.37 eV). The methyl transfer mechanism (eq 2a, Figure S3) for binding TMA on epoxidized GO is energetically less favorable (ΔE_c = −5.67 eV), making it less probable than the ethane release mechanism. TMA chemisorption on hydroxylated GO is predicted to proceed via the methane (CH_4) release pathway (eq 3a), in agreement with other −OH terminated substrates such as SiO_2, Al_2O_3, and TiO_2.[55] This reaction proceeds via a low barrier as well (ΔE_a= 0.09 eV, Figure S6) and produces a sizable energy gain (ΔE_r = −2.22 eV), rendering it accessible from both the kinetic and thermodynamic aspect. Dissociative TMA adsorption on the GO surface with a mixture of epoxy and hydroxyl groups will undergo either the methane- and ethane-release mechanism, depending on the actual surface composition. For the mixture model considered here (with 33% coverage) the ethane release mechanism is more likely to occur (ΔE_r = −4.72 vs −2.91 eV).

DFT calculations indicate a weaker TMA binding for the hydrogenated graphene (HG), compared to GO, but the binding is still stronger than for PG (Table 1). TMA physisorption on honeycomb and stirrup HG is of average strength (ΔE_p = −0.54 eV vs −0.44 eV). The dissociative binding of TMA is energetically favorable on both surfaces, whereas the stirrup configuration affords a somewhat stronger binding (ΔE_c = −2.23 eV vs −1.39 eV). The DFT results indicate that chemisorption proceeds most likely via the CH_4-release mechanism, as for the hydroxylated GO surface. However, different from the hydroxylated GO, dissociative binding of TMA (i.e., CH_4 formation) is preceded by a release of gaseous H_2 in order to facilitate the binding (eqs 3c−3d). This two-step chemisorption scheme is thermodynamically and kinetically accessible on both single-sided HG surfaces by being energetically downhill (ΔE_r = −1.69 eV and −0.95 eV) and having low activation barriers (ΔE_a = 0.18 and 0.17 eV, on stirrup and honeycomb respectively, see Figure S7a,b). However, compared to the various GO (see above), TMA chemisorption on HG surfaces is kinetically and thermodynamically less favorable, slowing down the TMA adsorption. This finding falls in line with the longer nucleation delay on HG in comparison to GO observed experimentally (Figure S2).

All the discussions are so far based on the zero-temperature gas-phase energies. To check the temperature and pressure effects on the reaction pathways, Gibbs free energy changes are also computed (Table 1), mimicking the typical ALD conditions during the precursor pulse (T = 100 °C and P = 13.3 Pa). As evident from the free energies, higher temperatures are expected to cause an overall weaker TMA physisorption (on all studied surfaces), most likely due to the decrease in the translational and rotational entropies of gaseous precursor molecules. This in turn would enhance the TMA desorption rate with increasing temperatures; however, this can be compensated by the simultaneous adsorption of multiple precursor molecules (as previously shown for TMA binding on Al_2O_3[56]). Besides, with more destabilized physisorbed species, the reaction energies are in general more negative at elevated temperatures (Table 1), rendering these reactions thermodynamically even more favored. It should also be noted that the energetically most feasible pathway for each considered surface remains the same as in the zero-temperature case, when temperature and pressure effects are also considered.

Considering the variety in the reaction mechanisms employed for the dissociative binding of TMA on diverse graphene surfaces, an overview is given in Figure 8. The most

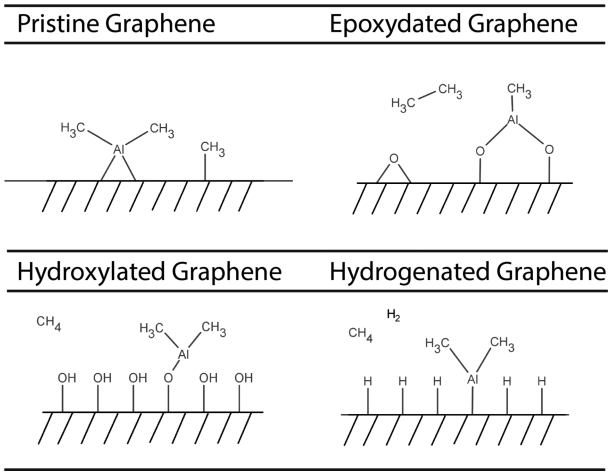

Figure 8. Schematic overview of the energetically most favorable TMA chemisorption mechanisms on pristine and functionalized graphene based on the PBE-D3-level calculations.

plausible pathway for hydrogenated graphene that combines H_2 and CH_4 release mechanisms is predicted to clean the hydrogen functionalities off the surface (typically three hydrogens per bound TMA molecule). In contrast, on the GO surfaces, the oxygen adatoms are predicted to stay on the graphene surface on all feasible pathways. This is the likely reason for the observed reversibility of the H_2 plasma treatment after Al_2O_3 ALD as opposed to O_2 plasma treaded graphene (see Figure 4).

4. CONCLUSIONS

In conclusion, uniform Al_2O_3 ALD growth on graphene was obtained by functionalizing graphene with a reversible H_2 plasma treatment, without deteriorating the graphene's electrical properties. The creation of C−H groups on the graphene surface during plasma treatment improved the adsorption of the ALD precursor TMA on graphene. This led to the formation of a closed uniform Al_2O_3 layer. On pristine graphene a closed film was not obtained due to the absence of dangling bonds and the resulting high activation barrier for TMA adsorption. DFT calculations confirmed the improved precursor adsorption on hydrogenated graphene. As for oxygen plasma treatments, the hydrogen plasma treatment led to the partial deterioration of the sp^2 hybridization of the graphene, which resulted in a drastic reduction in charge carrier mobility. Contrary to oxygen plasma functionalized graphene, for hydrogen plasma functionalized graphene this reduction in charge carrier mobility was fully recovered upon Al_2O_3 ALD. Subsequent annealing at 400 °C further improved the mobility to 152% of its initial value. DFT calculations showed that the recovery of charge carrier mobility can be explained by a

DOI: 10.1021/acs.chemmater.6b04368
Chem. Mater. 2017, 29, 2090−2100

reaction pathway, in which TMA adsorption on hydrogenated graphene proceeds via a CH_4 release mechanism preceded by the abstraction of H_2 from the surface, which recovers the sp^2 hybridization of graphene. The DFT predictions were confirmed by Raman spectroscopy. Factors that could explain the improvement of the charge carrier mobility of the graphene beyond its initial value are (1) the excellent barrier properties of the ALD Al_2O_3 after annealing, (2) screening of charged impurity by Al_2O_3, and (3) the removal of resist residues by the H_2 plasma treatment. Functionalization of graphene by H_2 plasma treatments is therefore an excellent way to enable direct ALD growth of thin uniform dielectric layers on graphene without deteriorating graphene's electrical properties.

■ ASSOCIATED CONTENT

Supporting Information

The Supporting Information is available free of charge on the ACS Publications website at DOI: 10.1021/acs.chemmater.6b04368.

Reversibility of plasma treatments, coverage of Al_2O_3 as a function of the ALD cycle number, motivation on choice of hydrogenated graphene models for DFT calculations, supporting figures, DFT calculations (structure, reaction pathways, etc.), and the influence of the SiO_2 substrate on the physisorption and chemisorption energies (PDF)

■ AUTHOR INFORMATION

Corresponding Author

*E-mail: a.a.bol@tue.nl.

ORCID

René H. J. Vervuurt: 0000-0002-6835-2323

Author Contributions

The manuscript was written through contributions of all authors. All authors have given approval to the final version of the manuscript.

Notes

The authors declare no competing financial interest.

■ ACKNOWLEDGMENTS

The authors would like to thank C. O. van Bommel, C. A. A. van Helvoirt, J. J. L. M. Meulendijks, and J. J. A. Zeebregts for technical assistance. Dr. H. Friedrich is acknowledged for providing access to the hall measurement system. This work is part of the research program of the Foundation for Fundamental Research on Matter (FOM), which is part of The Netherlands Organization for Scientific Research (NWO).

■ REFERENCES

(1) Morozov, S. V.; Novoselov, K. S.; Katsnelson, M. I.; Schedin, F.; Elias, D. C.; Jaszczak, J. A.; Geim, A. K. Giant Intrinsic Carrier Mobilities in Graphene and Its Bilayer. *Phys. Rev. Lett.* **2008**, *100*, 16602.

(2) Schwierz, F. Graphene Transistors. *Nat. Nanotechnol.* **2010**, *5*, 487−496.

(3) Wu, Y.; Jenkins, K. A.; Valdes-Garcia, A.; Farmer, D. B.; Zhu, Y.; Bol, A. A.; Dimitrakopoulos, C.; Zhu, W.; Xia, F.; Avouris, P.; Lin, Y.-M. State-of-the-Art Graphene High-Frequency Electronics. *Nano Lett.* **2012**, *12*, 3062−3067.

(4) Popinciuc, M.; Józsa, C.; Zomer, P. J.; Tombros, N.; Veligura, A.; Jonkman, H. T.; van Wees, B. J. Electronic Spin Transport in Graphene Field-Effect Transistors. *Phys. Rev. B: Condens. Matter Mater. Phys.* **2009**, *80*, 214427.

(5) Wang, X.; Tabakman, S. M.; Dai, H. Atomic Layer Deposition of Metal Oxides on Pristine and Functionalized Graphene. *J. Am. Chem. Soc.* **2008**, *130*, 8152−8153.

(6) Park, K. S.; Kim, S.; Kim, H.; Kwon, D.; Koo Lee, Y.-E.; Min, S.-W.; Im, S.; Choi, H. J.; Lim, S.; Shin, H.; Koo, S. M.; Sung, M. M. Wafer-Scale Single-Domain-like Graphene by Defect-Selective Atomic Layer Deposition of Hexagonal ZnO. *Nanoscale* **2015**, *7*, 17702−17709.

(7) Garces, N. Y.; Wheeler, V. D.; Gaskill, D. K. Graphene Functionalization and Seeding for Dielectric Deposition and Device Integration. *J. Vac. Sci. Technol., B: Nanotechnol. Microelectron.: Mater., Process., Meas., Phenom.* **2012**, *30*, 030801.

(8) Marichy, C.; Pinna, N. Carbon-Nanostructures Coated/decorated by Atomic Layer Deposition: Growth and Applications. *Coord. Chem. Rev.* **2013**, *257*, 3232−3253.

(9) Kim, J.; Jandhyala, S. Atomic Layer Deposition of Dielectrics for Carbon-Based Electronics. *Thin Solid Films* **2013**, *546*, 85−93.

(10) Fallahazad, B.; Kim, S.; Colombo, L.; Tutuc, E. Dielectric Thickness Dependence of Carrier Mobility in Graphene with HfO2 Top Dielectric. *Appl. Phys. Lett.* **2010**, *97*, 123105.

(11) Lee, B.; Park, S.; Kim, H.-C.; Cho, K.; Vogel, E. M.; Kim, M. J.; Wallace, R. M.; Kim, J. Conformal Al2O3 Dielectric Layer Deposited by Atomic Layer Deposition for Graphene-Based Nanoelectronics. *Appl. Phys. Lett.* **2008**, *92*, 203102.

(12) Lim, T.; Kim, D.; Ju, S. Direct Deposition of Aluminum Oxide Gate Dielectric on Graphene Channel Using Nitrogen Plasma Treatment. *Appl. Phys. Lett.* **2013**, *103*, 013107.

(13) Dlubak, B.; Kidambi, P. R.; Weatherup, R. S.; Hofmann, S.; Robertson, J. Substrate-Assisted Nucleation of Ultra-Thin Dielectric Layers on Graphene by Atomic Layer Deposition. *Appl. Phys. Lett.* **2012**, *100*, 173113.

(14) Farmer, D. B.; Chiu, H.-Y.; Lin, Y.-M.; Jenkins, K. A.; Xia, F.; Avouris, P. Utilization of a Buffered Dielectric to Achieve High Field-Effect Carrier Mobility in Graphene Transistors. *Nano Lett.* **2009**, *9*, 4474−4478.

(15) Alaboson, J. M. P.; Wang, Q. H.; Emery, J. D.; Lipson, A. L.; Bedzyk, M. J.; Elam, J. W.; Pellin, M. J.; Hersam, M. C. Seeding Atomic Layer Deposition of High- K Dielectrics on Epitaxial Graphene with Organic Self-Assembled Monolayers. *ACS Nano* **2011**, *5*, 5223−5232.

(16) Nayfeh, O. M.; Marr, T.; Dubey, M. Impact of Plasma-Assisted Atomic-Layer-Deposited Gate Dielectric on Graphene Transistors. *IEEE Electron Device Lett.* **2011**, *32*, 473−475.

(17) Young, M. J.; Musgrave, C. B.; George, S. M. Growth and Characterization of Al2O3 Atomic Layer Deposition Films on sp2 -Graphitic Carbon Substrates Using NO2 /Trimethylaluminum Pretreatment. *ACS Appl. Mater. Interfaces* **2015**, *7*, 12030−12037.

(18) Lee, B.; Mordi, G.; Kim, M. J.; Chabal, Y. J.; Vogel, E. M.; Wallace, R. M.; Cho, K. J.; Colombo, L.; Kim, J. Characteristics of High-K Al2O3 Dielectric Using Ozone-Based Atomic Layer Deposition for Dual-Gated Graphene Devices. *Appl. Phys. Lett.* **2010**, *97*, 043107.

(19) Jandhyala, S.; Mordi, G.; Lee, B.; Lee, G.; Floresca, C.; Cha, P.-R.; Ahn, J.; Wallace, R. M.; Chabal, Y. J.; Kim, M. J.; Colombo, L.; Cho, K.; Kim, J. Atomic Layer Deposition of Dielectrics on Graphene Using Reversibly Physisorbed Ozone. *ACS Nano* **2012**, *6*, 2722−2730.

(20) Shin, W. C.; Bong, J. H.; Choi, S.-Y.; Cho, B. J. Functionalized Graphene as an Ultrathin Seed Layer for the Atomic Layer Deposition of Conformal High-K Dielectrics on Graphene. *ACS Appl. Mater. Interfaces* **2013**, *5*, 11515−11519.

(21) Nourbakhsh, A.; Adelmann, C.; Song, Y.; Lee, C. S.; Asselberghs, I.; Huyghebaert, C.; Brizzi, S.; Tallarida, M.; Schmeißer, D.; Van Elshocht, S.; Heyns, M.; Kong, J.; Palacios, T.; De Gendt, S. Graphene Oxide Monolayers as Atomically Thin Seeding Layers for Atomic Layer Deposition of Metal Oxides. *Nanoscale* **2015**, *7*, 10781−10789.

(22) Park, Y. H.; Kim, M. H.; Kim, S. B.; Jung, H. J.; Chae, K.; Ahn, Y. H.; Park, J.-Y.; Rotermund, F.; Lee, S. W. Enhanced Nucleation of

DOI: 10.1021/acs.chemmater.6b04368
Chem. Mater. 2017, 29, 2090−2100

High-K Dielectrics on Graphene by Atomic Layer Deposition. *Chem. Mater.* **2016**, *28*, 7268−7275.
(23) Dingemans, G.; van de Sanden, M. C. M.; Kessels, W. M. M. Influence of the Deposition Temperature on the c-Si Surface Passivation by Al2O3 Films Synthesized by ALD and PECVD. *Electrochem. Solid-State Lett.* **2010**, *13*, H76.
(24) Elias, D. C.; Nair, R. R.; Mohiuddin, T. M. G.; Morozov, S. V.; Blake, P.; Halsall, M. P.; Ferrari, A. C.; Boukhvalov, D. W.; Katsnelson, M. I.; Geim, A. K.; Novoselov, K. S. Control of Graphene's Properties by Reversible Hydrogenation: Evidence for Graphane. *Science* **2009**, *323*, 610−613.
(25) Luo, Z.; Yu, T.; Kim, K.; Ni, Z.; You, Y.; Lim, S.; Shen, Z.; Wang, S.; Lin, J. Thickness-Dependent Reversible Hydrogenation of Graphene Layers. *ACS Nano* **2009**, *3*, 1781−1788.
(26) Blöchl, P. E. Projector Augmented-Wave Method. *Phys. Rev. B: Condens. Matter Mater. Phys.* **1994**, *50*, 17953−17979.
(27) Kresse, G.; Joubert, D. From Ultrasoft Pseudopotentials to the Projector Augmented-Wave Method. *Phys. Rev. B: Condens. Matter Mater. Phys.* **1999**, *59*, 1758−1775.
(28) Kresse, G.; Hafner, J. Ab Initio Molecular Dynamics for Liquid Metals. *Phys. Rev. B: Condens. Matter Mater. Phys.* **1993**, *47*, 558−561.
(29) Kresse, G.; Hafner, J. Ab Initio Molecular-Dynamics Simulation of the Liquid-Metal−amorphous-Semiconductor Transition in Germanium. *Phys. Rev. B: Condens. Matter Mater. Phys.* **1994**, *49*, 14251−14269.
(30) Kresse, G.; Furthmüller, J. Efficiency of Ab-Initio Total Energy Calculations for Metals and Semiconductors Using a Plane-Wave Basis Set. *Comput. Mater. Sci.* **1996**, *6*, 15−50.
(31) Kresse, G.; Furthmüller, J. Efficient Iterative Schemes for Ab Initio Total-Energy Calculations Using a Plane-Wave Basis Set. *Phys. Rev. B: Condens. Matter Mater. Phys.* **1996**, *54*, 11169−11186.
(32) Hohenberg, P.; Kohn, W. Inhomogeneous Electron Gas. *Phys. Rev.* **1964**, *136*, B864−B871.
(33) Kohn, W.; Sham, L. J. Self-Consistent Equations Including Exchange and Correlation Effects. *Phys. Rev.* **1965**, *140*, A1133−A1138.
(34) Perdew, J. P.; Burke, K.; Ernzerhof, M. Generalized Gradient Approximation Made Simple. *Phys. Rev. Lett.* **1996**, *77*, 3865−3868.
(35) Perdew, J. P.; Burke, K.; Ernzerhof, M. Generalized Gradient Approximation Made Simple [Phys. Rev. Lett. 77, 3865 (1996)]. *Phys. Rev. Lett.* **1997**, *78*, 1396−1396.
(36) Grimme, S.; Antony, J.; Ehrlich, S.; Krieg, H. A Consistent and Accurate Ab Initio Parametrization of Density Functional Dispersion Correction (DFT-D) for the 94 Elements H-Pu. *J. Chem. Phys.* **2010**, *132*, 154104.
(37) Karasulu, B.; Vervuurt, R.; Kessels, E.; Bol, A. A. Continuous and Ultrathin Platinum Films on Graphene Using Atomic Layer Deposition: A Combined Computational and Experimental Study. *Nanoscale* **2016**, *8*, 19829−19845.
(38) Gao, W. The Chemistry of Graphene Oxide. In *Graphene Oxide*; Springer International Publishing: Cham, 2015; pp 61−95.
(39) Criado, A.; Melchionna, M.; Marchesan, S.; Prato, M. The Covalent Functionalization of Graphene on Substrates. *Angew. Chem., Int. Ed.* **2015**, *54*, 10734−10750.
(40) Lin, Y.-C.; Lu, C.-C.; Yeh, C.-H.; Jin, C.; Suenaga, K.; Chiu, P.-W. Graphene Annealing: How Clean Can It Be? *Nano Lett.* **2012**, *12*, 414−419.
(41) C1s. http://xpssimplified.com/elements/carbon.php (accessed Jul 7, 2016).
(42) Eckmann, A.; Felten, A.; Mishchenko, A.; Britnell, L.; Krupke, R.; Novoselov, K. S.; Casiraghi, C. Probing the Nature of Defects in Graphene by Raman Spectroscopy. *Nano Lett.* **2012**, *12*, 3925−3930.
(43) Van Lam, D.; Kim, S.-M.; Cho, Y.; Kim, J.-H.; Lee, H.-J.; Yang, J.-M.; Lee, S.-M. Healing Defective CVD-Graphene through Vapor Phase Treatment. *Nanoscale* **2014**, *6*, 5639.
(44) Schwan, J.; Ulrich, S.; Batori, V.; Ehrhardt, H.; Silva, S. R. P. Raman Spectroscopy on Amorphous Carbon Films. *J. Appl. Phys.* **1996**, *80*, 440.
(45) Franklin, A. D.; Han, S.-J.; Bol, A. A.; Haensch, W. Effects of Nanoscale Contacts to Graphene. *IEEE Electron Device Lett.* **2011**, *32*, 1035−1037.
(46) Meric, I.; Dean, C. R.; Young, A. F.; Baklitskaya, N.; Tremblay, N. J.; Nuckolls, C.; Kim, P.; Shepard, K. L. Channel Length Scaling in Graphene Field-Effect Transistors Studied with Pulsed Current−Voltage Measurements. *Nano Lett.* **2011**, *11*, 1093−1097.
(47) Horiuchi, K.; Nakada, K.; Uchino, S.; Hashii, S.; Hashimoto, A.; Aoki, N.; Ochiai, Y.; Shimizu, M. Passivation Effects of Alumina Insulating Layer on C60 Thin-Film Field-Effect Transistors. *Appl. Phys. Lett.* **2002**, *81*, 1911.
(48) Ryu, S.; Liu, L.; Berciaud, S.; Yu, Y.-J.; Liu, H.; Kim, P.; Flynn, G. W.; Brus, L. E. Atmospheric Oxygen Binding and Hole Doping in Deformed Graphene on a SiO2 Substrate. *Nano Lett.* **2010**, *10*, 4944−4951.
(49) Chen, F.; Xia, J.; Ferry, D. K.; Tao, N. Dielectric Screening Enhanced Performance in Graphene FET. *Nano Lett.* **2009**, *9*, 2571−2574.
(50) Hoex, B.; Schmidt, J.; Pohl, P.; van de Sanden, M. C. M.; Kessels, W. M. M. Silicon Surface Passivation by Atomic Layer Deposited Al2O3. *J. Appl. Phys.* **2008**, *104*, 044903.
(51) Oh, I.-K.; Tanskanen, J.; Jung, H.; Kim, K.; Lee, M. J.; Lee, Z.; Lee, S.-K.; Ahn, J.-H.; Lee, C. W.; Kim, K.; Kim, H.; Lee, H.-B.-R. Nucleation and Growth of the HfO 2 Dielectric Layer for Graphene-Based Devices. *Chem. Mater.* **2015**, *27*, 5868−5877.
(52) Kim, K.; Lee, H.-B.-R.; Johnson, R. W.; Tanskanen, J. T.; Liu, N.; Kim, M.-G.; Pang, C.; Ahn, C.; Bent, S. F.; Bao, Z. Selective Metal Deposition at Graphene Line Defects by Atomic Layer Deposition. *Nat. Commun.* **2014**, *5*, 4781.
(53) Elliott, S. D. Atomic-Scale Simulation of ALD Chemistry. *Semicond. Sci. Technol.* **2012**, *27*, 074008.
(54) Elliott, S. D.; Dey, G.; Maimaiti, Y.; Ablat, H.; Filatova, E. A.; Fomengia, G. N. Modeling Mechanism and Growth Reactions for New Nanofabrication Processes by Atomic Layer Deposition. *Adv. Mater.* **2016**, *28*, 5367−5380.
(55) Potts, S. E.; Kessels, W. M. M. Energy-Enhanced Atomic Layer Deposition for More Process and Precursor Versatility. *Coord. Chem. Rev.* **2013**, *257*, 3254−3270.
(56) Weckman, T.; Laasonen, K. First Principles Study of the Atomic Layer Deposition of Alumina by TMA−H2O-Process. *Phys. Chem. Chem. Phys.* **2015**, *17*, 17322−17334.

DOI: 10.1021/acs.chemmater.6b04368
Chem. Mater. 2017, 29, 2090−2100